

Representation Recycling for Streaming Video Analysis

Can Ufuk Ertenli¹, Ramazan Gokberk Cinbis^{1*}, Emre Akbas^{1*}

¹Department of Computer Engineering, Middle East Technical University (METU), Ankara, Turkey

Abstract—We present StreamDEQ, a method that aims to infer frame-wise representations on videos with minimal per-frame computation. Conventional deep networks do feature extraction from scratch at each frame in the absence of ad-hoc solutions. We instead aim to build streaming recognition models that can natively exploit temporal smoothness between consecutive video frames. We observe that the recently emerging implicit layer models provide a convenient foundation to construct such models, as they define representations as the fixed-points of shallow networks, which need to be estimated using iterative methods. Our main insight is to distribute the inference iterations over the temporal axis by using the most recent representation as a starting point at each frame. This scheme effectively recycles the recent inference computations and greatly reduces the needed processing time. Through extensive experimental analysis, we show that StreamDEQ is able to recover near-optimal representations in a few frames’ time and maintain an up-to-date representation throughout the video duration. Our experiments on video semantic segmentation, video object detection, and human pose estimation in videos show that StreamDEQ achieves on-par accuracy with the baseline while being more than 2-4x faster.

Index Terms—Implicit layer models, streaming video understanding, object detection, semantic segmentation, human pose estimation.

I. INTRODUCTION

Modern convolutional deep networks excel at numerous recognition tasks. It is commonly observed that deeper models tend to outperform their shallower counterparts [1], [2]. Due to the sequential dependencies across the layers, however, increasing the network depth results in longer processing times. While the increase in inference duration can be acceptable for various offline recognition problems, it is typically of concern for many streaming video analysis tasks. For example, in perception modules of autonomous systems, it is not only necessary to keep up with the frame rate but also desirable to minimize the computational burden of each recognition component to reduce the hardware requirements. Similarly, in large-scale video analysis tasks, small changes in per-frame computations can lead to significant cumulative cost differences.

The most naive way to use deep networks in video analysis tasks is to apply the deep network independently at each frame to extract features (Fig. 1a). Although this scheme is inefficient in the sense that it does not exploit the temporal smoothness in the video, its ease of application makes this scheme ubiquitous in industrial applications and many academic works

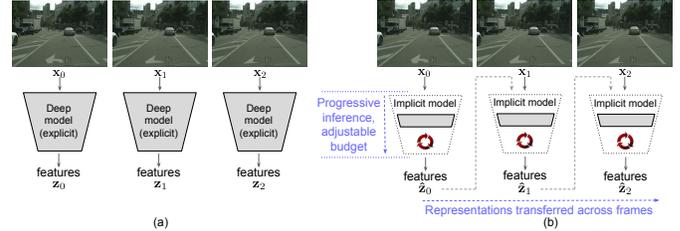


Fig. 1: (a) Naive per-frame processing. (b) The proposed scheme allows reusing features continuously during the stream and dynamically adjusting the number of inference iterations, where at each time step the current frame’s representation progressively improves over the iterations.

as well [3], [4], [5], [6]. As an alternative to the naive approach, various techniques have been proposed to speed up the inference in streaming video analysis. A widely studied idea is to apply a large model to selected *key frames* and then either interpolate its features to the intermediate frames [7], [8] or apply a smaller model to them [9], [10]. However, such approaches come with several potential complications, *e.g.* costs & errors of the introduced motion estimators [7], [8], maintenance of the compability across the key and non-key frame representations, dependency on video training data, *etc.* It is also noteworthy that several models, *e.g.* [11], [12], rely on forward **and** backward flow estimates, making them less suitable for streaming recognition problems due to non-causal processing.

A related approach is to select a subset of each frame to process. These methods typically aim to identify the most informative regions in the input [13], [14], [15]. For static images, the region selection process can continue until the model becomes confident about its predictions. However, when applied to videos, such subset selection strategies share shortcomings similar to approaches relying on flow-based intra-frame prediction approximations. The inputs change over time, therefore the models have to choose between relying on optical flow to warp the rest of the features or to omit them entirely, which may result in obsolete representations over time [8].

In this context, we envision a model which exploits the temporal smoothness¹ between consecutive video frames by re-using the features of the previous frame. Ideally, we are looking for two desirable properties: (i) natively exploit video

¹We do not imply a mathematical definition of smoothness and only emphasize that the differences between neighboring frames are small.

*Equal contribution for senior authorship.

smoothness for compute-efficient inference, avoiding from-scratch compute at each frame and need for ad-hoc solutions such as flow-based feature transfer, (ii) ensure that the representation quality improves over the compute time spent within a frame, enabling progressive inference for the downstream task (Fig. 1b). These two requirements jointly open doors to important flexibilities for real-time and large-scale systems. For instance, the system may take an action based on early inference results (e.g. emergency braking in an autonomous vehicle), dynamically change compute time based on the instantaneous availability of compute resources, or reduce compute costs on scenes with quick representation convergence.

Our insight is to leverage the power of the recently introduced *implicit layer models*, pioneered by the work on Deep Equilibrium Model (DEQ) [16] and Multiscale Deep Equilibrium Model (MDEQ) [17] to achieve these properties. They offer a fundamentally different alternative to deep neural networks: (M)DEQ shows that by using the fixed points of a network as the representation, one can gain the representation power of deep models using a network with *only a few layers*. The potential of DEQ to eliminate long chains of computations over network layers, therefore, renders it an attractive candidate towards building efficient streaming recognition models.

While DEQ provides a way to learn deep representations using shallow networks, the test-time inference process involves iterative root-finding algorithms such as Newton’s or quasi-Newton methods, e.g. Broyden’s method [18], to estimate the fixed point of the network. One can also leverage fixed point iterations by repeatedly applying the same layer to its output to again find the fixed point, which would be analogous to the rolled-out version of DEQ. Since each iteration can be interpreted as an increment in the network depth in both cases, its computational budget is adjustable and DEQ effectively constructs deep networks for inference. However, they can still suffer from run-time costs as in explicit deep networks.

Our main insight is the potential to speed up the inference process by exploiting the temporal smoothness across neighboring frames in videos. We observe that the fully estimated MDEQ representation of a frame can be used for obtaining the approximate representations of the following frames, using only a few inference iterations. We further develop the idea and show that even without fully estimating the representation at any time step, the representation can be kept up-to-date by running the inference iterations over the iteration steps *and* video time steps in a continuous manner. The final scheme, starting from scratch, accumulates and transfers the extracted information throughout the video duration. We, therefore, refer to the proposed method as Streaming DEQ, or StreamDEQ for short.

The main difference between standard DEQ and our StreamDEQ is illustrated in Fig. 2. While DEQ typically requires a large number of inference iterations, StreamDEQ enables inference with only a few iterations per frame by leveraging the relevance of the most recent frame’s representation. At the start of a new video stream, or after a major content

change (e.g. a shot change), StreamDEQ quickly adapts to the video in a few frames, much like a person adapting her/his focus and attention when watching a new video. In the following frames, it continuously updates the representation to adapt to minor changes (e.g. objects moving, entering, or exiting the scene). We further introduce a stochastic version of StreamDEQ, where the number of iterations per frame is not fixed and determined randomly at each frame. We show that this stochastic version outperforms all other versions of StreamDEQ, i.e. the versions using Broyden’s method or unrollings of the model in every downstream task.

Overall, StreamDEQ provides a simple and *lean* solution to streaming recognition both with implicit layer models and the explicit versions of said implicit models, where a single model naturally performs cost-effective recognition without relying on external inputs and heuristics, such as optical flow [19], post-processing methods (Seq-NMS [20] or tubelet re-scoring [21], [11]). In contrast to the common requirements of RNN-based video models, e.g. [22], StreamDEQ does not require fixing the number of iterations during training and does not even require (costly-to-annotate) video training data, thanks to the equilibrium-based scheme. Our method also maintains the causality of the system and executes in a continuous manner. We also note that it allows dynamic time budgeting; the duration of the inference process can be tuned on-the-fly by a controller, depending on the instantaneous compute system load, which can be a desirable feature in real-world scenarios.

We verify the effectiveness of the proposed method through extensive experiments on video semantic segmentation, video object detection and human pose estimation in videos. Our experimental results show that StreamDEQ recovers near-optimal representations at much lower inference costs. More specifically, on the ImageNet-VID video object detection task, StreamDEQ converges to the mAP scores of 69.5 and 70.3 using only 4 and 8 inference iterations per frame, respectively. In comparison, the standard DEQ inference scheme yields only 8.2 and 32.6 mAP scores using 4 and 8 iterations, respectively. Similarly, on the Cityscapes semantic segmentation task, using StreamDEQ instead of the standard DEQ inference scheme improves the converged streaming mIoU score from 42.3 to 77.9 when 4 inference iterations are used per frame and from 73.2 to 80.0 when 8 iterations are used per frame. Finally, for human pose estimation in videos using the MPII dataset, we achieve 89.4 and 89.9 PCKh with StreamDEQ, whereas the standard DEQ inference scheme achieves 42.7 and 79.5 PCKh when we perform 4 and 8 iterations, respectively.

Our contributions are as follows: (i) We introduce a new inference scheme based on DEQ that can be applied to streaming videos to improve processing speeds drastically while maintaining a high level of performance. (ii) To the best of our knowledge, we provide the first attempt at applying implicit layer models to videos and specifically streaming videos. (iii) We empirically show that the fixed points for neighboring video frames are near each other; therefore, previous frames’ fixed points provide a good starting point for

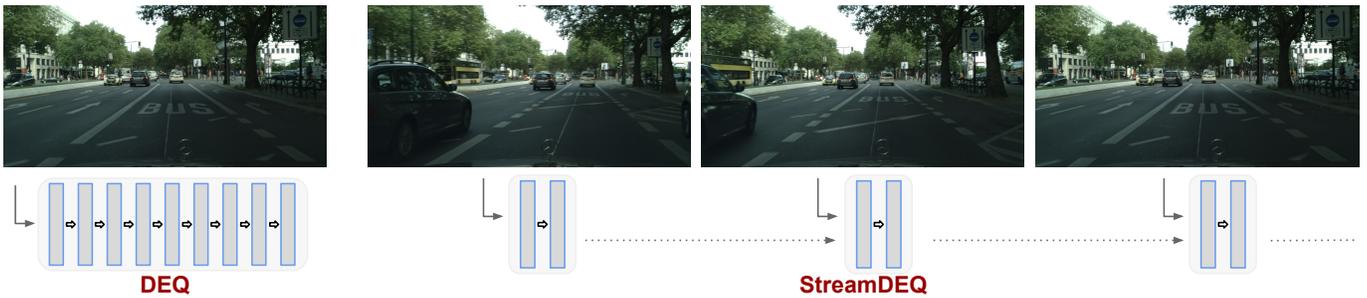


Fig. 2: Our method, StreamDEQ, exploits the temporal smoothness between successive frames and extracts features via a small number of solver iterations, starting from the previous frame’s representation as initial solution. StreamDEQ accumulates and transfers the extracted information continuously over successive frames; effectively sharing computations across video frames in a causal manner.

the upcoming frames. (iv) In addition to applying the implicit layers to streaming videos, we also show the effectiveness of our method beyond implicit models in more general terms based on the idea of feature re-use. (v) We propose two new variations based on DEQ to estimate the fixed point of the current frame using unrollings of the network where the number of unrollings can either be fixed or selected stochastically during training.

This paper is an extension of our previous work [23]. Firstly, we extend the inference scheme of StreamDEQ beyond iterative root-finding methods and incorporate fixed point iteration based unrolling scheme. This version of StreamDEQ, which we call Unrolled StreamDEQ or shortly UR-StreamDEQ (Section III-C) is much faster and more accurate in all our experiments offering speed-ups of up to $4\times$ while also providing accuracy gains of up to $5\times$ in some settings. We also propose a stochastic variant of Unrolled StreamDEQ, namely, Stochastically Unrolled StreamDEQ (SUR-StreamDEQ), where the number of iterations is randomly selected on-the-fly during training. We show that this version of StreamDEQ further improves the performance using fewer frames. Importantly, we provide insight into why the StreamDEQ scheme works by showing empirical evidence. Furthermore, we added an entirely new section (Section IV-C) which describes our experiments on human pose estimation, as a completely new task. Overall, this extended version presents more than 100 extra experiments over our previous work. Additionally, we provide an extended literature review to cover recent developments especially in the field of implicit layer models as well as a new subsection on human pose estimation in videos. To avoid confusion, from here onward, we refer to the StreamDEQ version using iterative root-finding methods as Implicit StreamDEQ (IL-StreamDEQ).

In the rest of the paper, we first provide an overview of related work in Section II. In Section III, we describe our inference scheme and how we apply StreamDEQ to streaming videos. In Section IV, we present the details of our experimental setup and demonstrate the results of our extensive experiments to verify the effectiveness of our method

on challenging datasets. Finally, we conclude with a summary of our work in Section V.

II. RELATED WORK

Here, we summarize efficient video processing methods, video object detection, segmentation, and human pose estimation models. Furthermore, we discuss saliency-based techniques for image and video processing. Finally, we overview implicit models and introduce some important application areas.

A. Efficient Video Processing and Inference

There have been many efforts to improve video processing efficiency to reach real-time processing speeds. Most of these works take a system-oriented approach [24], [25], [26]. For example, Carreira et al. [24] develop an efficient parallelization scheme over multiple GPUs and process different parts of a model in separate GPUs to improve efficiency while sacrificing accuracy due to frame delays. Narayanan et al. [25] propose a novel scheduling mechanism that efficiently schedules and divides forward and backward passes over multiple GPUs. In another work, Li et al. [26] use a dynamic scheduler that skips frame(s) when the delays build up to the point where it would be impossible to calculate the results of the next frame in the allotted time.

We note that works on low-cost network designs, such as MobileNets [27], [28] and low-resolution networks [29], [30], are also relevant. Such efforts are valuable primarily for replacing network components with more compute-friendly counterparts. However, the advantages of such techniques can also be limited due to natural trade-offs between speed and performance [31], as the lower-cost network components tend to have lower expressive power. Nevertheless, one can easily incorporate low-cost model design principles into DEQ or StreamDEQ models, thanks to the architecture-agnostic definition of implicit layer models. While such efforts may bring reductions in inference wall-clock time, they are outside the scope of our work.

B. Video Semantic Segmentation

Semantic segmentation is a costly, spatially dense prediction task. Due to this specific nature of the task, its application to videos remains relatively limited. Most works rely on exploiting temporal relations between frames using methods such as feature warping [32], [9], [33], [34], feature propagation [35], [36], [37], feature aggregation [38], and knowledge distillation [39], [40], [41] to reduce the computational cost.

Gadde et al. [32] propose warping features of the previous frame at different depths based on optical flow. Xu et al. [9] evaluate regions of the input frame and decide whether to warp the features with a cheap flow network or use the large segmentation model based on a confidence score. Huang et al. [33] keep a moving average over time by combining the segmentation maps from the current frame with the warped map from the previous frame. Jain et al. [34] warp high-quality features from the last key frame and fuse them with lower-quality features calculated on the current frame to make predictions.

Shelhamer et al. [35] propose an adaptive method that schedules updates to the multi-level feature map so that features of layers with smaller changes are carried forward (without any transformation). Li et al. [36] introduce an adaptive key frame scheduling method based on the deviation of low-level features compared to the previous key frame. If the deviation is small, the features are propagated with spatially variant convolution. Liang et al. [37] apply the full model on key frames and propose to adaptively choose the depth of the network at each non-key frame.

Hu et al. [38] use a set of shallow networks, each calculating features of consecutive frames starting from scratch. Then, these features are aggregated at the current frame with an attention-based module. Liu et al. [39], [40] propose to use an expensive network during training and applies knowledge distillation on a student network to cut the test-time compute costs. On the other hand, Habibian et al. [41] use a teacher network on key frames, and through knowledge distillation, guide the student network to learn feature differences that are combined with the key frame features to simulate the teacher on non-key frames.

In contrast to all these approaches, the proposed StreamDEQ scheme directly leverages the similarities across video frames, without requiring any ad-hoc video handling strategies, as a way to adapt the implicit layer inference mechanism to efficient streaming video analysis.

C. Video Object Detection

Most modern video object detection methods exploit temporal information to improve the accuracy and efficiency. To this end, optical flow [7], [42], [11], [12], feature aggregation [42], [43], [44], [45] and post-processing techniques [20], [21] are prominently used.

Zhu et al. [7] introduce Deep Feature Flow (DFF) and use optical flow estimates to warp features on selected key frames to intermediate frames for increased efficiency. Zhu et al. [42] also propose Flow-Guided Feature Aggregation (FGFA) which

uses optical flow to warp features of nearby frames to the current frame and aggregates these features adaptively based on feature similarity. Kang et al. [11] create links between objects through time (tubelets) from the predictions calculated with optical flow across a video linking objects through time and apply tubelet re-scoring to keep detections of high confidence. Wang et al. [12] add an instance level calibration module to FGFA [42] and combine them to generate better predictions.

Bertasius et al. [43] sample features from neighboring support frames via deformable convolution that learns object offsets between frames and aggregates these features over these frames. Wu et al. [44] focus on linking object proposals in a video according to their semantic similarities. Chen et al. [45] propose a model aggregating local and global information with a long-range memory.

Another common way to improve performance is to apply a post-processing method. For example, Han et al. [20] introduce Seq-NMS to exploit temporal consistency by constructing a temporal graph to link objects in adjacent frames. With a similar idea, Kang et al. [21] generate tubelets by combining single image detections through the video and use a tracker to re-score the tubelets during post-processing to improve temporal consistency.

D. Human Pose Estimation in Videos

Most previous work on human pose estimation in videos operates in a single-frame manner [46]. However, utilizing temporal information can be valuable for human pose estimation in videos as it can improve the model robustness and/or efficiency. Using recurrent models [47], [48], [49], optical flow [50], [51] and/or temporal convolutions [52], [5] are some of the common efforts.

Gkioxari et al. [47] chain predictions in time by utilizing a recurrent network for improved performance. Lin et al. [48] accumulate pose information temporally with an LSTM block by feeding the concatenation of the previous pose predictions to regress 3D body joints on the current frame. Artacho et al. [49] incorporate an LSTM module into their model and feed it with the heatmaps from the previous video frames along with the current frame's heatmap and generate the heatmap for the final prediction.

Pfister et al. [50] generate heatmaps for all frames individually and warp them using optical flow to later pool them on the current frame to make its predictions. Xiao et al. [51] use optical flow and a tracker that performs greedy matching to shift and track the poses in time.

Pavlo et al. [52] use dilated temporal convolutions over a sequence of 2D keypoints to capture long term information and generate 3D keypoint detections. Duan et al. [5] uses a two-stage pose estimation where the first step is to detect bounding boxes. Using those bounding boxes, the model estimates poses on each frame. Finally, these predictions are stacked to create 3D heatmap volumes which are then processed with temporal convolutions for classification.

E. Saliency Based Techniques

To reduce computational cost, another viable approach is to select important regions in an image and process only those small patches [13], [14], [15], [53]. Video extensions of these models also exist [54], [55], [8], [56], [57], [58], [59].

Mnih et al. [13] and Ba et al. [14] model human eye movements by capturing *glimpses* from images with a recurrent structure and process those glimpses at each step. Cordonnier et al. [15] propose selecting the most important regions to process by first processing a downsampled version of the image. Liu et al. [53] stops processing for regions with high-confidence predictions at an earlier stage.

Bazzani et al. [54] and Denil et al. [55] approach video processing in a human-like manner where the model *looks at* a different patch around the objects of interest at each frame and tracks them. Zhu et al. [8] take a key frame based approach. At each key frame the method processes the entire input, and at intermediate frames, it updates the feature maps partially based on temporal consistency. Rhee et al. [56] identify changing regions between frames and re-use the features of the static parts on non-key frames. Habibian et al. [57] introduce skip-convolutions where the model determines changing locations via frame difference and computes convolutions only on some part of each frame. Patchwork [58] uses a Q-learning based policy to select a sub-window in each frame and combines the sub-window features with the rest of the features via an attention mechanism. SALISA [59] focuses on an intelligent downsampling method that *magnifies* important regions in each frame and reduces the frame’s resolution.

F. Implicit Layer Models

Implicit layer models have seen a recent surge of interest and have been outstanding at tackling numerous tasks. DEQ [16] is a new addition to the implicit model family aimed at solving sequence modeling tasks. DEQ reformulates the fixed point solving problem as root finding and utilizes an iterative root-finding algorithm to find a solution. Multiscale Deep Equilibrium Models (MDEQ) [17] are the extension of the base DEQ to image-based models where there are multiple fixed points for different feature scales.

Since the introduction of DEQ and MDEQ, there have been many efforts to improve and exploit implicit layer models. Huang et al. [60] propose re-using the fixed point across training iterations, however with the drawback of having to stay in full-batch mode for the training. Bai et al. [61] suggest a new initialization scheme that is realized through a small network. Furthermore, inferring information from the last few iterations reduces the number of solver iterations required for convergence. Pal et al. [62] propose mixing implicit models with explicit models. Usually, implicit models are initialized from scratch, *i.e.* from a random point or zero, to iteratively reach the equilibrium point. Instead, this method first utilizes an explicit model to calculate a “better” starting point for the implicit model, resulting in better performance and faster inference.

Several works have shown the versatility of the implicit layer models as a replacement of explicit ones. Examples of previously explored applications include optical flow estimation [63], normalizing flows [64], feature refinement [65], and Feature Pyramid Networks [66].

Even though DEQs offer a new avenue for research that can potentially surpass explicit models, they are susceptible to several problems. First of all, DEQ models grow increasingly unstable as the training progresses, and they are brittle to architectural choices meaning even minor modifications may harm the model’s convergence [67]. Furthermore, their backward passes are especially costly [68], [69]. Bai et al. [67] propose adding a Jacobian regularization term to mitigate these issues to improve model training. Geng et al. [68] and Fung et al. [69] focus on the backward pass to make it less costly. Both works [68], [69] utilize the Neumann series expansion and show that calculating inexact gradients using low-level expansions are sufficient during training.

III. PROPOSED METHOD

In this section, we first give an overview of DEQ and then present the details of our Implicit StreamDEQ method. We finally present its unrolling based variants, *i.e.* Unrolled and Stochastically Unrolled StreamDEQ.

A. DEQ Overview

Weight-tied networks are models where some or all layers share the same weights [70], [71]. A DEQ is essentially a weight-tied network with only one shallow block. DEQ leverages the fact that continuously applying the same layer to its output tends to guide the output to an equilibrium point, *i.e.* a fixed point. Let \mathbf{x} represent the model’s input, \mathbf{z}^* the equilibrium point, f_θ the applied shallow block, and the superscript $[i]$ each iteration, then an explicit weight-tied network can be described as

$$\lim_{i \rightarrow \infty} \mathbf{z}^{[i+1]} = \lim_{i \rightarrow \infty} f_\theta(\mathbf{z}^{[i]}; \mathbf{x}) \equiv f_\theta(\mathbf{z}^*; \mathbf{x}) = \mathbf{z}^*. \quad (1)$$

Each iteration in Eq. (1) is an unrolling of the model, akin to recurrent neural networks (RNNs), and this scheme is called the fixed point iteration. DEQ’s fundamental difference from a standard weight-tied model is that the model is represented by an implicit equation, and the fixed point is found by employing root-finding algorithms in both forward and backward passes, by rewriting Eq. (1) as follows:

$$g_\theta(\mathbf{z}; \mathbf{x}) = f_\theta(\mathbf{z}; \mathbf{x}) - \mathbf{z} = 0 \implies \mathbf{z}^* = \text{RootFind}(g_\theta; \mathbf{x}). \quad (2)$$

Using Eq. (2), the gradients for a given loss ℓ can be computed directly only by using the final output [16]:

$$\frac{\partial \ell}{\partial (\cdot)} = \frac{\partial \ell}{\partial \mathbf{z}^*} (I - J_{f_\theta}(\mathbf{z}^*))^{-1} \frac{\partial f_\theta(\mathbf{z}^*; \mathbf{x})}{\partial (\cdot)}, \quad (3)$$

where $J_{f_\theta}(\mathbf{z}^*)$ is the Jacobian matrix at \mathbf{z}^* .

DEQ uses Broyden’s method [18] to calculate the root of Eq. (2). In this setting, the accuracy of the solution depends on the number of Broyden iterations [61], [67], [65]. While more

iterations yield better accuracy, they increase computational cost.

DEQs have been successfully adapted to computer vision tasks with the introduction of Multiscale Deep Equilibrium Models (MDEQ) [17]. MDEQ is a multiscale model where each scale is driven to equilibrium together with other scales in the same manner as DEQs. Broyden iterations start with $\mathbf{z}^{[0]} = \mathbf{0}$ and continue N times to obtain the final solution, $\mathbf{z}^{[N]}$. N is set to 26 for ImageNet classification and 27 for Cityscapes semantic segmentation in MDEQ [17].

B. Streaming DEQ

In this section, we present the StreamDEQ framework. All numerical results presented in this section use the iterative root-finding methods. The explanations on unrolling and stochastic unrolling variants of StreamDEQ are later provided in the following subsection.

Let \mathbf{X} be a $H \times W \times 3 \times T$ dimensional tensor representing a video where T is the temporal dimension. We represent the frame at time t with \mathbf{x}_t which is a $H \times W \times 3$ tensor. It should be noted that we primarily target videos with temporal continuity, without too frequent shot changes.

To process a video, DEQ can be applied to each video frame \mathbf{x}_t to obtain \mathbf{z}_t^* , the representation of that frame. This amounts to running the Broyden solver for N iterations starting from $\mathbf{z}_t^{[0]} = \mathbf{0}$ for each frame.

However, we know a priori that transitions between subsequent video frames are typically smooth, *i.e.* $\mathbf{x}_{t-1} \sim \mathbf{x}_t$. From this observation, we hypothesize that the corresponding fixed points, *i.e.* representations \mathbf{z}_{t-1}^* and \mathbf{z}_t^* , are likely to be similar. Therefore, the representation of the previous frame can be used effectively as a starting point for inferring the representation of the current frame. To validate this hypothesis, we run an analysis on the ImageNet-VID [72] dataset using the ImageNet pretrained MDEQ model. We assume that at each frame \mathbf{x}_t , we have access to the reference representation, \mathbf{z}_{t-1}^* , of the previous frame. Reference representations are obtained by running the MDEQ model until convergence ($N = 26$ iterations). At each frame, we use the reference representation of the previous frame as the starting point of the solver,

$$\mathbf{z}_t^{[0]} = \mathbf{z}_{t-1}^*, \quad (4)$$

and run the solver for various but small numbers of iterations, M . To analyze the amount of change in representations over time, we use an ImageNet-pretrained model since ImageNet representations are known to be useful in many transfer learning tasks. In Fig. 3, we show the squared Euclidean distance between $\mathbf{z}_t^{[M]}$ and \mathbf{z}_t^* for various M values when the solver starts as in Eq. (4). Dashed lines correspond to the squared Euclidean distance between MDEQ’s reference and M -iteration based representations. Notice that the dashed black line indicating the 0 iterations case shows the distance of the reference representation to the initial point.

From the results presented in Fig. 3, we observe that after starting from the reference representation of the previous frame and not performing any iterations, the approximate

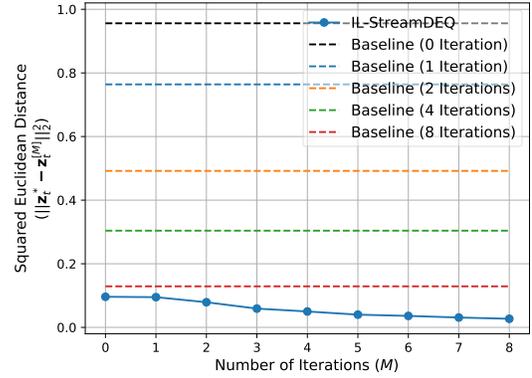


Fig. 3: Squared Euclidean approximation error as a function of inference steps, when the solver is initialized with the reference representation of the preceding frame.

representation is already more similar to the reference one than starting from scratch and performing 8 iterations (the solid blue line starts below the red dashed line even at 0 iterations). We also observe that when we initialize the solver with the preceding frame’s fixed point, the inference process converges towards the reference representation in under 8 iterations. Our findings noticeably agree with those in Pal et al. [62], which show that good initializations of the solver generally lead to better convergence for single images, and indicate that the fixed point of the preceding frame is a good starting point for calculating the fixed point of the following frame in videos.

Next, we examine the case where the inference method is given access to the reference representations only at certain frames. To simulate this case, for each video clip, we compute the reference representation only at the first frame \mathbf{x}_0 , *i.e.* \mathbf{z}_0^* . In the following frames, we initialize the solver with the estimated representation of the preceding frame and run the solver for M iterations. That is,

$$\mathbf{z}_1^{[0]} = \mathbf{z}_0^* \text{ and } \mathbf{z}_t^{[0]} = \mathbf{z}_{t-1}^{[M]}. \quad (5)$$

We present the results of this scheme for $M \in \{1, 2, 4, 8\}$ in Fig. 4. To ensure that the analysis is performed on the same annotated frame with differing video lengths, we use the following evaluation strategy. Suppose that the test video clip has an annotated frame at time n . When we start StreamDEQ’s inference at frame $n - t$, run it up to frame n and evaluate it at frame n , we record its squared Euclidean distance at the horizontal axis equal to t . For example, the point at $t = 10$ on the blue curve in Fig. 4 corresponds to the squared Euclidean distance obtained when IL-StreamDEQ is started 10 frames before the evaluation frame.

We observe that starting with the reference representation on the initial frame is still useful, but for longer clips, its effect diminishes. Still, this scheme helps us maintain a stable performance even after several frames. For example, starting with the reference representation and then applying $M = 2$ iterations per frame throughout the following 20 frames yields a representation closer to the reference representation of the

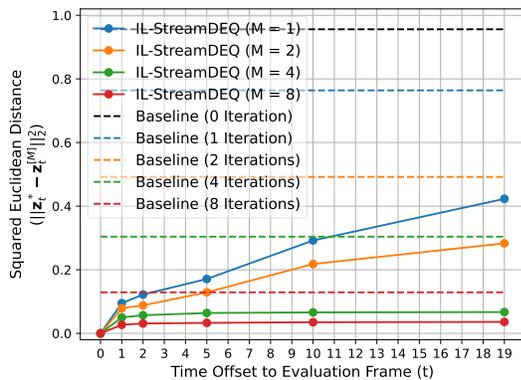


Fig. 4: Distance between the reference representations and IL-StreamDEQ estimations for varying number of iterations, when IL-StreamDEQ is initialized with reference representations on the first frame.

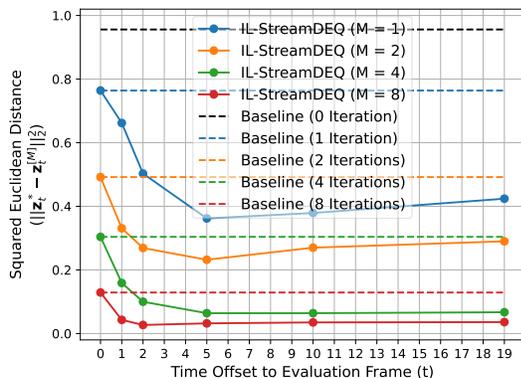


Fig. 5: Distance between the reference representations and IL-StreamDEQ estimations, when IL-StreamDEQ is initialized with just zeros on the first frame.

final frame than the one given by baseline DEQ inference with 4 solver iterations. This result shows that the M -step inference scheme is able to keep up with the changes in the scene by starting from a good initial point.

While this scheme can provide efficient inference on novel frames, we would still need the reference representations of the initial frames, or key frame(s), which would share the same problems with key frame based video recognition approaches, *e.g.* [7], [9], [10]. To address this problem, we further develop the idea, and hypothesize that we can start from scratch (*i.e.* all zeros), do a limited number of iterations per frame, and pass the representation to the next frame as the starting point. That is,

$$\mathbf{z}_0^{[0]} = 0 \text{ and } \mathbf{z}_t^{[0]} = \mathbf{z}_{t-1}^{[M]}. \quad (6)$$

We present the corresponding representation distance results in Fig. 5. The representation distances to the reference representations stabilize in 20 frames. The converged distance values (in 20 frames) are similar to those in the previous scheme (Eq. (5)). Additionally, the initial representations have relatively large distances, but these differences get smaller as new

frames arrive. We call this scheme StreamDEQ. *This scheme avoids heavy processing in any of the frames and completely avoids the concept of key frames.* The number of iterations can be tuned, which allows controlling the time/accuracy trade-off easily. Therefore, the inference iterations can be run as much as the time budget allows. An illustration of the StreamDEQ scheme is given in Fig. 6.

To understand the asymptotic behavior of StreamDEQ better, we present two additional empirical results. In the first one, we investigate whether the consecutive frames converge to fixed points that are in close proximity in the feature space. For this purpose, we visualize the t-SNE [73] embeddings of pairs of consecutive frame representations as found by the Broyden solver for each M value, starting from zero initializations, for 15 different videos. The results are shown in Fig. 7. We observe that for $M = 0$, all 30 frames start at a similar location but then, each consecutive frame pair takes a different path. Importantly, we see that each frame in a pair follow a similar trajectory especially during early iterations, *e.g.*, $M \leq 5$ and then due to the differences between consecutive frames, the paths move away from each other while still being widely separated from any other frame pair for $M = 26$. This is the idea to which StreamDEQ relies upon indicating that there is strong correlation between consecutive frame pairs' representations during all iterations.

Secondly, we look into the change of residual ($\|z^{[M+1]} - z^{[M]}\| / \|z^{[M]}\|$) for varying M values, inspired from the still image convergence analysis in Bai et al. [17]. We perform a similar study on videos using IL-StreamDEQ and present the results for 1, 2, 4, 8, and 21 iterations per frame in Fig. 8. When $M = 1$, a frame change occurs at every iteration on the horizontal axis; for $M = 2$, a frame change occurs at every second iteration on the horizontal axis and finally, $M = 21$ corresponds to the still image case, as in MDEQ [17]. The general trend we see coincides with our intuition given in Fig. 5 in the sense that the change of residual drops to lower values as the number of iterations per frame increases, *i.e.* the number of frames is smaller. For lower numbers of iterations per frame, the trend is still downwards and we observe convergent behavior. Importantly, we clearly see the effect of the frame changes at their respective intervals but even that does not induce a divergent behavior. The points at which a frame change occurs also follow a downward trend, suggesting that the adverse effect of prematurely moving to the next frame is quickly mitigated in the iterations that follow.

C. Unrolled & Stochastically Unrolled Streaming DEQ

In addition to using the root-finding formulation, we can also formulate our scheme as the fixed point iteration problem from Eq. (1), *i.e.* the weight-tied setting. This allows us to approach the fixed point solving problem through the more standard explicit point of view. This only changes how the fixed point is found while keeping everything else the same, *e.g.* f_θ . We refer to this version as Unrolled StreamDEQ (UR-StreamDEQ).

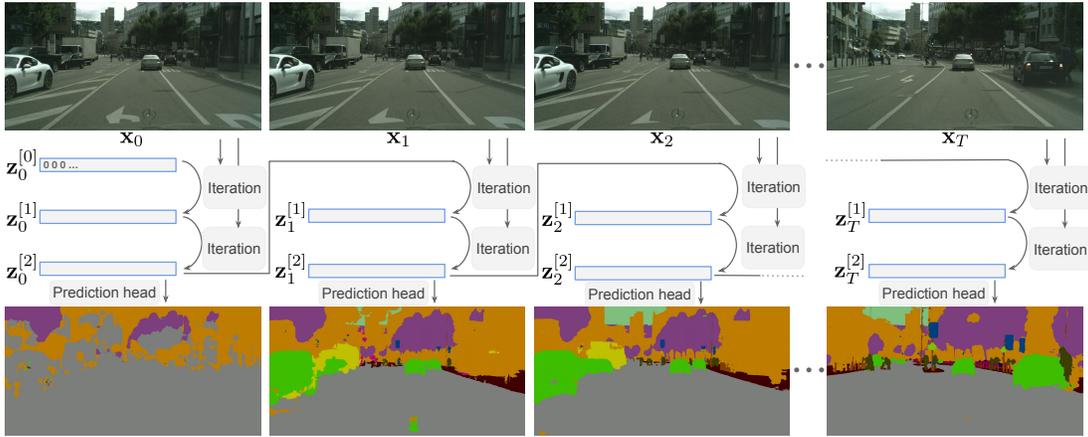


Fig. 6: StreamDEQ applied to a streaming video, using two iterations per frame. The process is initialized with zeros in the very first frame ($\mathbf{z}_0^{[0]} = \mathbf{0}$) and with the most recent representation ($\mathbf{z}_t^{[0]} = \mathbf{z}_{t-1}^{[2]}$) afterwards. This scheme effectively recycles all recent computations for time-efficient inference and therefore, allows approximating a long inference chain (*i.e.* a deep network) by a few inference steps (*i.e.* a few layers) throughout the video stream. Note that the term *iteration* refers to Broyden iterations for IL-StreamDEQ, and unrollings for (S)UR-StreamDEQ. IL-StreamDEQ predictions are shown.

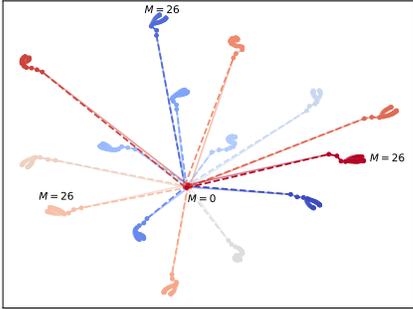


Fig. 7: t-SNE visualizations of inference processes. Each color represents a consecutive frame pair. (Best viewed in color)

As the only difference between these two versions is the solution procedure, our previous arguments regarding the *smoothness* of videos and the nature of fixed points of neighboring frames are still valid for UR-StreamDEQ. Thus, we can still argue that starting with either the reference representations (Eq. (5)) or from scratch (Eq. (6)), UR-StreamDEQ eventually reaches a stable condition where its representations yield comparable performance with that of the reference representation, for the downstream task. We confirm this claim with our experimental findings in Section IV. Note that when considering Eq. (5) and Eq. (6) in the context of UR-StreamDEQ, the superscripts represent the number of unrollings instead of the Broyden iterations where we use a constant number of unrollings. This is equivalent to applying the same layer repeatedly for a fixed number of times to its output while injecting the input frame into the model every time.

We aim to further improve UR-StreamDEQ by randomizing the number of unrollings during training. Importantly, this

modification only affects the training phase: for each batch of training frames, instead of using a fixed number of unrollings (*e.g.* 20), we set the number of unrollings uniformly and at random (*e.g.* between 1 and 20), while keeping the test-time inference the same. We refer to this variant as Stochastically Unrolled StreamDEQ (SUR-StreamDEQ).

We note that most previous works [16], [17], [66], [65], [63] report observations on the advantages of using Broyden iterations over explicit weight-tied versions, typically in terms of achieving quicker convergence. In Section IV, we empirically demonstrate that this is not always the case and fewer than 20 unrollings (*i.e.* fixed point iterations) are sufficient to reach an equilibrium in most scenarios. In most cases, even when the model is unrolled a few times per frame in streaming evaluation, we observe performances on the same level as the variants using blackbox root-finding methods, with a noticeably smaller computational burden. We finally note that our video-inference findings are in line with the recent observations on unrolled DEQ inference on images reported in Fung et al. [69].

IV. EXPERIMENTAL RESULTS

We show the effectiveness of our method on three streaming video analysis tasks: object detection, semantic segmentation and human pose estimation. For each task, we evaluate all three StreamDEQ variants, denoted with the prefixes *IL*-, *UR*-, and *SUR*-. To remind briefly: *IL* uses the Broyden solver; both *UR* and *SUR* use explicit unrolling (*i.e.* repeated application of the model on its output), *SUR* is trained with a random number of unrollings. In the following, we provide details on the datasets we used, the training and inference setups, and present our results for each task. We conducted all our experiments in PyTorch [74].

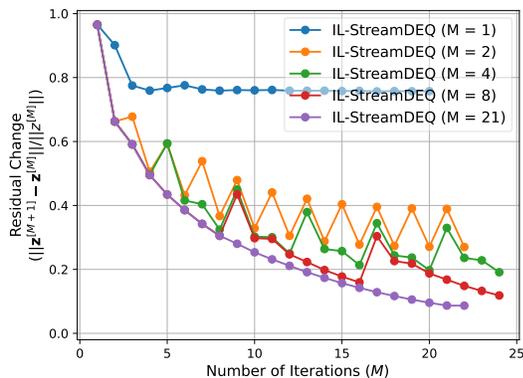


Fig. 8: Change of residual per iteration for differing numbers of iterations on streaming videos.

A. Video Semantic Segmentation

1) *Experimental Setup*: We use the Cityscapes semantic segmentation dataset [75], focusing on its subset of 5K finely annotated images. The dataset is divided into train, validation, and test sets, each containing 2975, 500, and 1525 images, respectively. They correspond to frames extracted from video clips where each annotated image is the 20th frame of its respective clip. To evaluate over videos, we use these clips up to the 20th frame, which has fine annotations, and evaluate on that frame.

For IL-StreamDEQ, we use the pretrained MDEQ segmentation model from the MDEQ paper [17] and do not perform any training. However, for (S)UR-StreamDEQ, an off-the-shelf, pretrained model does not exist. Therefore, we train the models with their respective unrolling settings for 480 epochs with 0.01 initial learning rate with cosine scheduling following the training setup used in the MDEQ paper [17], initially starting from the ImageNet-pretrained model. Note that we train the model with still images and do not incorporate temporal information during the training phase.

We follow the evaluation setup and hyperparameters used in MDEQ [17], perform the evaluation on Cityscapes `val` and report *mean intersection over union* (mIoU) results. The architecture of the MDEQ consists of 4 residual blocks of different scales where each block contains convolution layers, group normalization, and ReLU activation. For further details, we refer the reader to MDEQ [17].

2) *Results*: We evaluate IL-StreamDEQ using our final StreamDEQ formulation (*i.e.* Eq. (6)), where we initialize the solver from scratch, *i.e.* with all zeros, and apply IL-StreamDEQ. The results are shown in Fig. 9. As the videos progress, one might expect that the Broyden solver cannot keep up with the changing scenes. However, we observe that even after 20 frames, the accuracy does not drop. Additionally, the impact of this method is more evident for the lower numbers of iterations. For example, performing 1 iteration on every frame without our method would only yield an mIoU score of 2.2. However, IL-StreamDEQ obtains an mIoU score of 44.9 in 10 frames, providing an improvement of

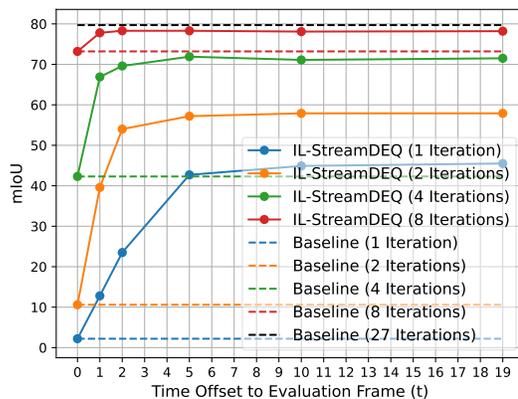


Fig. 9: IL-StreamDEQ semantic segmentation results (in mIoU) on the Cityscapes dataset as a function of solver iterations when the first frame representation is initialized with zeros.

over 20 \times . For 8 iterations, IL-StreamDEQ is able to obtain 78.1 mIoU in 10 frames, whereas the non-streaming baseline achieves only 73.2 mIoU. Moreover, we also investigate the case where we use the reference representations of the first frame to initialize the solver and apply IL-StreamDEQ then on (Eq. (5)). We observe that the converged mIoU values (at larger frame offsets) are similar in this case compared to Fig. 9. This is similar to our observation comparing Fig. 4 and Fig. 5. Further details regarding this experiment can be found in the supplementary material. Therefore, we conclude that the initial point where we start the solver becomes less crucial as the video streams and the performance stabilizes at some value higher than in the non-streaming case.

We illustrate the results of IL-StreamDEQ qualitatively in Fig. 10. With 2 iterations, while the DEQ baseline produces poor results, IL-StreamDEQ starts to yield accurate predictions as early as the 2nd frame. Afterwards, IL-StreamDEQ improves its predictions with every new frame producing a clear picture while the DEQ baseline struggles since it has to compute everything from scratch with each frame.

We similarly evaluate the streaming recognition performance of UR-StreamDEQ and SUR-StreamDEQ schemes for varying number of iterations per frame, and present the results in Fig. 11 and Fig. 12, respectively. Overall, we observe that (S)UR-StreamDEQ performs better than IL-StreamDEQ. For example, after the first 1-2 frames are processed, especially SUR-StreamDEQ reaches its performance level at the end of the video, meaning that it is able to adapt to the changing scenes faster while starting out from 38.4 mIoU in the 1 iteration case as opposed to IL-StreamDEQ starting out from 2.2 mIoU after the first frame. One other observation we have is that in terms of final performances at the end of the videos, SUR-StreamDEQ comes first (*e.g.* 71.2 mIoU for 2 iterations per frame), followed by UR-StreamDEQ (*e.g.* 67.2 mIoU for 2 iterations per frame), and finally comes IL-StreamDEQ (*e.g.* 57.9 mIoU for 2 iterations per frame).

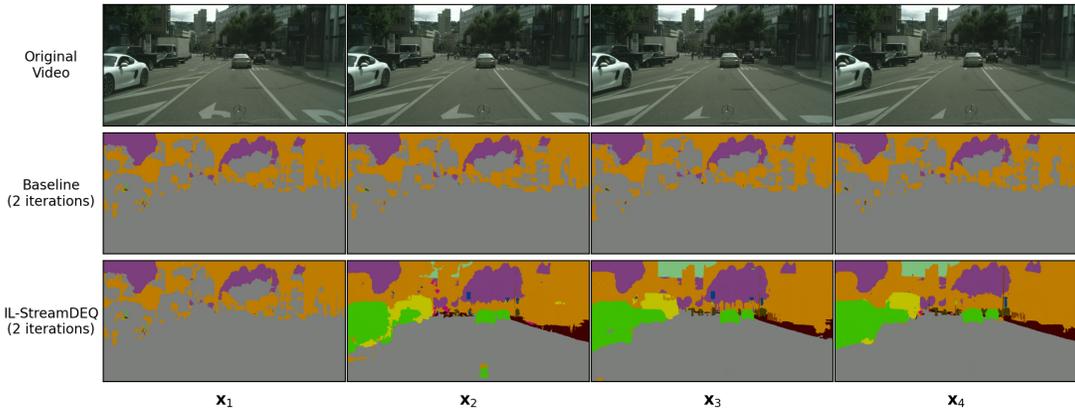


Fig. 10: Qualitative comparison of the baseline with StreamDEQ with 2 iterations on the Cityscapes dataset. (Please refer to the supplementary material for a more detailed version of this analysis.)

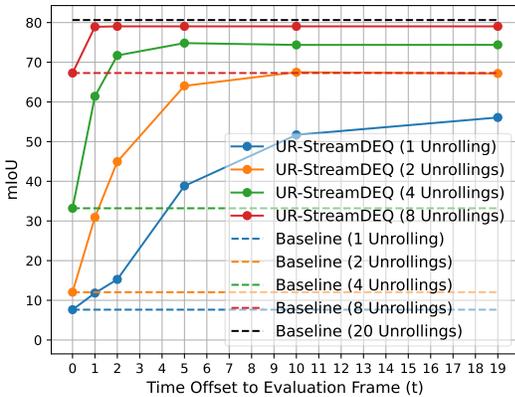


Fig. 11: mIoU results of UR-StreamDEQ for various number of iterations after initialization with zeros from the beginning of a clip on the Cityscapes dataset.

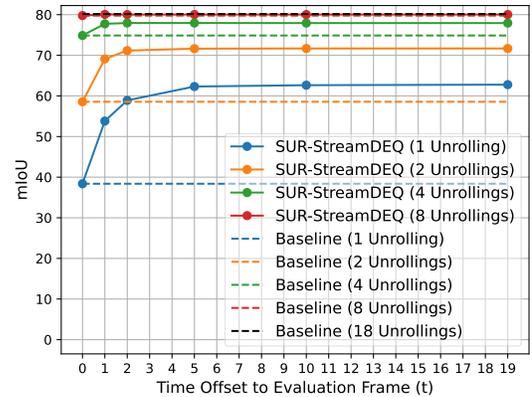


Fig. 12: mIoU results of SUR-StreamDEQ for various number of iterations after initialization with zeros from the beginning of a clip on the Cityscapes dataset.

One interesting matter is the performance comparison of UR-StreamDEQ and SUR-StreamDEQ, especially for the lower number of unrollings. We see that SUR-StreamDEQ is again attaining its final performance before UR-StreamDEQ for all numbers of iterations in fewer frames, *e.g.* for 1 iteration per frame, after the first frame, UR-StreamDEQ achieves 7.8 mIoU while SUR-StreamDEQ beats this value by a wide margin achieving 38.8 mIoU. We attribute this to the model’s robustness to the noise introduced by the lower number of iterations during training as well as to the accumulation of information through time.

We examine the effects of increasing the number of iterations on inference speed in Table I. Our method does not introduce any computation overhead other than the time it takes to store the previous frame’s fixed point representation. Therefore, we observe a linear increase in compute times as the number of iterations increases. IL-StreamDEQ with 4 iterations achieves an mIoU score of 71.5 at 530 ms per image. MDEQ with 4 iterations can only achieve 42.3 mIoU. Even though IL-StreamDEQ performs better than MDEQ, we

find that even in the single-frame setting, unrolled variants of StreamDEQ are superior to IL-StreamDEQ both in terms of speed and accuracy as indicated by Table I. We provide additional inference results with videos on our project page (<https://ufukertenli.github.io/streamdeq/>).

We also study the effects of shot changes for the video semantic segmentation task where we effectively connect two different clips together either within the same context or an entirely different context. We refer interested readers to the supplementary material for the results.

B. Video Object Detection

1) *Experimental Setup*: For the video object detection task, we evaluate our method on the ImageNet-VID dataset [72], a challenging video dataset with fast-moving objects, camera movement, and motion blur. We utilize the MMDetection [76] and MMTracking [77] frameworks for the implementation.

The ImageNet-VID dataset consists of 3862 training and 555 validation videos from 30 classes that are a subset of the 200 classes of the ImageNet-DET dataset. The frames and

TABLE I: Performances and inference times of StreamDEQ variants on three streaming video tasks: semantic segmentation, object detection and human pose estimation.

Model	# iterations*	Cityscapes		ImageNet-VID		MPII	
		mIoU	FPS	mAP@50	FPS	PCKh	FPS
IL-StreamDEQ	1	45.5	4.3	9.1	10.3	47.9	22.3
UR-StreamDEQ		56.1	6.3	59.4	23.2	73.8	48.2
SUR-StreamDEQ		62.8		65.1		79.6	
IL-StreamDEQ	2	57.9	2.9	39.5	9.2	70.1	19.2
UR-StreamDEQ		67.2	4.9	64.1	17.4	78.6	27.4
SUR-StreamDEQ		71.7		68.8		86.8	
IL-StreamDEQ	4	71.5	1.9	50.4	6.2	83.6	14.4
UR-StreamDEQ		74.4	3.2	65.7	11.6	86.2	22.3
SUR-StreamDEQ		77.9		69.5		89.4	
IL-StreamDEQ	8	78.2	1.1	54.8	3.5	86.2	12.2
UR-StreamDEQ		79.0	1.9	67.2	6.8	84.7	19.6
SUR-StreamDEQ		80.0		70.3		89.9	
IL-StreamDEQ Baseline**	27	79.7	0.3	55.0	1.2	85.6	2.7
UR-StreamDEQ Baseline**	20	80.6	0.9	70.8	3.1	90.4	10.6
SUR-StreamDEQ Baseline**		80.2		70.2		90.2	

* The number of Broyden iterations for StreamDEQ and number of unrollings for (S)UR-StreamDEQ.

** The marked baselines operate on a single-frame basis.

annotations for each video are available at a rate of 25-30 FPS per video. Note that the ImageNet-DET dataset consists only of images rather than videos. We follow the widely used protocol [42], [12], [78], [44], [45] and train our model on the combination of ImageNet-VID and ImageNet-DET datasets using the 30 overlapping classes. We use a mini-batch size of 4, distributed to 4 NVIDIA A100 GPUs. We resize each image to have a shorter side of 600 pixels and train the model for a total of 7 epochs in 3 stages. We initialize the learning rate to 0.01 and divide it by 10 after epochs 2 and 5. We test the model on ImageNet-VID val and report mAP@50 scores following the common practice.

We adopt Faster R-CNN [79] by replacing its ResNet backbone with the MDEQ model. To incorporate multi-level representations, we also use a Feature Pyramid Network (FPN) [80] module after MDEQ. Without any additional modifications, we directly utilize the model while keeping the model hyperparameters and remaining architectural details the same as other Faster R-CNN models with ResNet backbones. We only modify the number of channels for the FPN module to match that of MDEQ. We start the training with the ImageNet pretrained MDEQ model [17].

To train IL-StreamDEQ we use 26 iterations per frame, following the ImageNet classification experiments in MDEQ [17]. (S)UR-StreamDEQ uses the same architecture and training details with the only difference being the solver. We keep the number of unrollings fixed at 20 for UR-StreamDEQ while SUR-StreamDEQ follows the previous principle whereby we choose a random number between 1 and 20 during training for each mini batch.

Unlike many video object detection models [42], [78], [45], we train our models in the causal single-frame setting, meaning we do not use any temporal information for improved training.

2) *Results*: To the best of our knowledge, this is the first time an implicit model has been used for a video object detection task. We achieve 55.0, 70.8, and 70.2 mAP@50 with IL-StreamDEQ, UR-StreamDEQ, and SUR-StreamDEQ, respectively on ImageNet-VID val (see Table I). We are aware that Faster R-CNN with ResNet-50 backbone yields 70.7 mAP@50 off-the-shelf; however, Faster R-CNN is highly optimized to perform well with ResNet backbones. Yet, we use the same setting with an MDEQ without any parameter optimization, as our focus is not on constructing an MDEQ-based state-of-the-art video object detector. We believe there is room for improvement in detector design and tuning details.

We run IL-StreamDEQ, UR-StreamDEQ, and SUR-StreamDEQ models with different numbers of iterations. Due to space constraints, we only present the full results obtained with SUR-StreamDEQ and refer readers to the supplementary material for the details regarding the other models. We present the results of this experiment in Fig. 13.

Our first observation is that the baseline single-frame performances of (S)UR-StreamDEQ are higher than IL-StreamDEQ. Furthermore, even with 1 unrolling per frame, SUR-StreamDEQ attains about 60 mAP@50 after 20 frames. We again discover that the scores stabilize at a value proportional to the number of unrollings. SUR-StreamDEQ starts with a strong 15.5 mAP@50 even after one frame with 1 unrolling. We suggest that this is due to the robustness to noise we introduce to SUR-StreamDEQ by the randomness in the number of unrollings during training.

SUR-StreamDEQ is able to sustain its performance with any number of unrollings once the initial frames are processed, e.g. the performance of the model with 2 unrollings per frame reaches to 68.8 mAP@50 after 10 frames and does not drop from its maximum value after 20 frames. Comparing SUR-StreamDEQ with UR-StreamDEQ, we see that the randomness added during training improves the performance which is

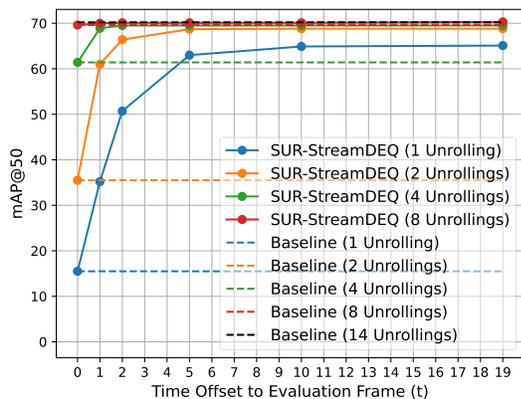


Fig. 13: mAP@50 results of SUR-StreamDEQ for various number of iterations after initialization with zeros from the beginning of a clip on the ImageNet-VID dataset.

demonstrated in Table I. After 20 frames, SUR-StreamDEQ outperforms UR-StreamDEQ with all numbers of unrollings by 3-5 mAP@50. While UR-StreamDEQ only learns about 20 unrollings per frame, SUR-StreamDEQ has knowledge about a frame’s representation after any number of unrollings. Therefore, it is able to adapt to more challenging situations (noisy representations), and its performance improves drastically. Furthermore, SUR-StreamDEQ maintains its performance even after 20 frames with as low as 2 unrollings per frame.

Notice that the single-frame performance of SUR-StreamDEQ uses 14 unrollings. Other StreamDEQ variants use the maximum number of iterations/unrollings that they use during training to make full use of their potential. However, since the number of unrollings per frame is not deterministic with SUR-StreamDEQ, we observe its best single-frame performance using 14 unrollings, achieving 70.2 mAP@50. For example, with 20 unrollings, the score drops to 69.9 mAP@50. The variations between different numbers of unrollings are minor but still, this shows the effectiveness of the stochasticity by saving 6 unrollings per frame with a 0.3 performance improvement even in the single-frame setting.

Additionally, SUR-StreamDEQ catches up to its single-frame performance with both 4 and 8 unrollings per frame on streaming videos. Usually, the single-frame performance of any Stream-DEQ model acts as an upper bound to its streaming video performance. This makes sense since the models become accustomed to still images from the training phase, yet, we introduce motion during streaming evaluation. Thus, the performance should degrade slightly due to the injection of moving pictures at each time step. It is interesting to note that SUR-StreamDEQ manages to optimize in such a way that it can tolerate the “noise” coming from the shifting objects between successive frames and achieves 70.3 mAP@50 after 20 frames. This is 0.1 more than its single-frame baseline. This demonstrates that even though the performance only marginally improves, with the stochasticity we add to the

model during training, the model becomes more effective in the low unrolling scenarios by learning diverse levels of representation complexities.

C. Human Pose Estimation in Videos

1) *Experimental Setup*: We train and evaluate StreamDEQ on the MPII dataset [81] for human pose estimation in videos. We implement StreamDEQ with the MMPose [82] framework.

MPII dataset contains 25k images collected from YouTube videos with over 40k people performing a variety of actions. Even though MPII is an image dataset, it also contains the frames from the YouTube videos, but these frames are unlabeled. We make use of these unlabeled frames when evaluating StreamDEQ on videos, however, only calculate the performance on the annotated frames.

The architecture consists of the pretrained MDEQ as the backbone and the top down heatmap head from Xiao et al. [51]. Our overall structure also follows that of Xiao et al. [51] with MDEQ replacing the backbone. We train the model with the ground-truth bounding boxes, in the single-frame setting without any temporal information for 210 epochs using a batch size of 256 with an initial learning rate of 10^{-4} which we divide by 10 after epochs 170 and 200. All StreamDEQ versions share the same architectural and training details. We train IL-StreamDEQ with 26 Broyden iterations per frame, UR-StreamDEQ with 20 unrollings per frame, and finally SUR-StreamDEQ with a random number of unrollings between 1 and 20 chosen before processing each mini-batch. We report our results using the Percentage of Correct Keypoints (PCKh) metric. Furthermore, unlike many common pose detectors [83], [84], [85], we do not perform flip testing which would improve the test time accuracy but would also increase computational costs. More details about the training procedure and the hyperparameters we use for training will be available with our code.

2) *Results*: For this task, we again train the three StreamDEQ variants. We only provide an overview of the results in Table I and the full results for SUR-StreamDEQ in Fig. 14 and refer readers to the supplementary material for the details regarding IL-StreamDEQ and UR-StreamDEQ.

The results of this experiment align with our previous experiments, in that, we see that the performance of the model improves rapidly after the first few frames. Again due to the stochasticity we introduce to SUR-StreamDEQ, it produces predictions with over 50 PCKh even after the first frame for all numbers of iterations. Furthermore, performing 4 iterations per frame versus 8 iterations per frame only makes a small difference as the performance saturates at about 90 PCKh for SUR-StreamDEQ.

Compared to UR-StreamDEQ, SUR-StreamDEQ is able to outperform its deterministic counterpart by 3-6 PCKh during streaming evaluation for any number of iterations (see Table I) following the pattern in our evaluations with the other downstream tasks.

The model from Xiao et al. [51] achieves 88.2 PCKh with a ResNet-50 backbone with flip testing in the single-frame

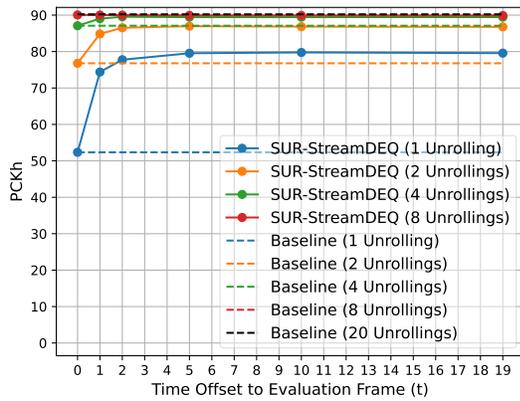


Fig. 14: PCKh results of SUR-StreamDEQ for various number of iterations after initialization with zeros from the beginning of a clip on the MPII dataset.

setting [82]. On the other hand, SUR-StreamDEQ achieves a single-frame performance of 90.2 PCKh without any test time augmentations. SUR-StreamDEQ outperforms the baseline model in terms of accuracy and speed for both the streaming and single-frame scenarios with streaming performances being superior for more than 16 PCKh in the 2 iteration per frame setting while being almost 1.5 times faster.

V. CONCLUSIONS

In this paper, we proposed StreamDEQ, an efficient streaming video application of the multiscale implicit deep model, MDEQ. To the best of our knowledge, this is the first large-scale video application of DEQs. Furthermore, we introduced two explicit variants of StreamDEQ. We showed that our models could start from scratch (*i.e.* all zeros) and efficiently update their representations to reach near-optimal representations as the video streams. We validated this claim on video semantic segmentation, video object detection, and human pose estimation tasks with thorough experiments.

StreamDEQ models present a viable approach for both real-time video analysis and off-line large-scale methods. StreamDEQ is not specific to segmentation, object detection, or pose estimation and can be used as a drop-in replacement for most other structured prediction problems on streaming videos (action recognition, depth estimation etc.) as long as the prediction task involves an iterative fixed point solution procedure. StreamDEQ works as is in most cases without needing additional tuning demonstrating the versatility of StreamDEQ.

In addition, StreamDEQ is architecture-agnostic, meaning its architecture (f_θ) can be tuned to fit any criteria. The approach proposed in this paper can easily be used in conjunction with current and future developments.

ACKNOWLEDGMENT

The numerical calculations were partially performed at TUBITAK ULAKBIM, High Performance and Grid Computing Center (TRUBA) and METU Robotics and AI Tech-

nologies Research Center (ROMER) resources. Dr. Cinbis is supported by a Google Faculty Research Award. Dr. Akbas is supported by the BAGEP Award of the Science Academy, Turkey.

REFERENCES

- [1] K. He, X. Zhang, S. Ren, and J. Sun, "Deep residual learning for image recognition," 2016, pp. 770–778.
- [2] G. Huang, Z. Liu, L. Van Der Maaten, and K. Q. Weinberger, "Densely connected convolutional networks," 2017, pp. 4700–4708.
- [3] Q. Zhou, X. Li, L. He, Y. Yang, G. Cheng, Y. Tong, L. Ma, and D. Tao, "Transvod: end-to-end video object detection with spatial-temporal transformers," 2022.
- [4] H. Wang, J. Tang, X. Liu, S. Guan, R. Xie, and L. Song, "Ptseformer: Progressive temporal-spatial enhanced transformer towards video object detection." Springer, 2022, pp. 732–747.
- [5] H. Duan, Y. Zhao, K. Chen, D. Lin, and B. Dai, "Revisiting skeleton-based action recognition," 2022, pp. 2969–2978.
- [6] G. Ponimatkin, N. Samet, Y. Xiao, Y. Du, R. Marlet, and V. Lepetit, "A simple and powerful global optimization for unsupervised video object segmentation," in *Proceedings of the IEEE/CVF Winter Conference on Applications of Computer Vision*, 2023, pp. 5892–5903.
- [7] X. Zhu, Y. Xiong, J. Dai, L. Yuan, and Y. Wei, "Deep feature flow for video recognition," 2017, pp. 2349–2358.
- [8] X. Zhu, J. Dai, L. Yuan, and Y. Wei, "Towards high performance video object detection," 2018, pp. 7210–7218.
- [9] Y.-S. Xu, T.-J. Fu, H.-K. Yang, and C.-Y. Lee, "Dynamic video segmentation network," 2018, pp. 6556–6565.
- [10] M. Liu, M. Zhu, M. White, Y. Li, and D. Kalenichenko, "Looking fast and slow: Memory-guided mobile video object detection," *arXiv:1903.10172*, 2019.
- [11] K. Kang, H. Li, J. Yan, X. Zeng, B. Yang, T. Xiao, C. Zhang, Z. Wang, R. Wang, X. Wang *et al.*, "T-cnn: Tubelets with convolutional neural networks for object detection from videos," *IEEE Transactions on Circuits and Systems for Video Technology*, vol. 28, no. 10, pp. 2896–2907, 2017.
- [12] S. Wang, Y. Zhou, J. Yan, and Z. Deng, "Fully motion-aware network for video object detection," 2018, pp. 542–557.
- [13] V. Mnih, N. Heess, A. Graves, and K. Kavukcuoglu, "Recurrent models of visual attention," Z. Ghahramani, M. Welling, C. Cortes, N. Lawrence, and K. Q. Weinberger, Eds., vol. 27. Curran Associates, Inc., 2014.
- [14] J. Ba, V. Mnih, and K. Kavukcuoglu, "Multiple object recognition with visual attention," 2015.
- [15] J.-B. Cordonnier, A. Mahendran, A. Dosovitskiy, D. Weissenborn, J. Uszkoreit, and T. Unterthiner, "Differentiable patch selection for image recognition," 2021, pp. 2351–2360.
- [16] S. Bai, J. Z. Kolter, and V. Koltun, "Deep equilibrium models," 2019.
- [17] S. Bai, V. Koltun, and J. Z. Kolter, "Multiscale deep equilibrium models," 2020.
- [18] C. G. Broyden, "A class of methods for solving nonlinear simultaneous equations," *Mathematics of computation*, vol. 19, no. 92, pp. 577–593, 1965.
- [19] B. K. Horn and B. G. Schunck, "Determining optical flow," *Artificial intelligence*, vol. 17, no. 1-3, pp. 185–203, 1981.
- [20] W. Han, P. Khorrami, T. L. Paine, P. Ramachandran, M. Babaeizadeh, H. Shi, J. Li, S. Yan, and T. S. Huang, "Seq-nms for video object detection," *arXiv:1602.08465*, 2016.
- [21] K. Kang, W. Ouyang, H. Li, and X. Wang, "Object detection from video tubelets with convolutional neural networks," 2016, pp. 817–825.
- [22] Y. Lu, C. Lu, and C.-K. Tang, "Online video object detection using association lstm," 2017, pp. 2344–2352.
- [23] C. U. Ertenli, E. Akbas, and R. G. Cinbis, "Streaming multiscale deep equilibrium models." Springer, 2022, pp. 189–205.
- [24] J. Carreira, V. Patraucean, L. Mazare, A. Zisserman, and S. Osindero, "Massively parallel video networks," 2018, pp. 649–666.
- [25] D. Narayanan, A. Harlap, A. Phanishayee, V. Seshadri, N. R. Devanur, G. R. Ganger, P. B. Gibbons, and M. Zaharia, "Pipedream: generalized pipeline parallelism for dnn training," in *Proceedings of the 27th ACM Symposium on Operating Systems Principles*, 2019, pp. 1–15.
- [26] M. Li, Y.-X. Wang, and D. Ramanan, "Towards streaming perception." Springer, 2020, pp. 473–488.

- [27] A. G. Howard, M. Zhu, B. Chen, D. Kalenichenko, W. Wang, T. Weyand, M. Andreetto, and H. Adam, "Mobilenets: Efficient convolutional neural networks for mobile vision applications," *arXiv:1704.04861*, 2017.
- [28] M. Sandler, A. Howard, M. Zhu, A. Zhmoginov, and L.-C. Chen, "Mobilenetv2: Inverted residuals and linear bottlenecks," 2018, pp. 4510–4520.
- [29] M. Liu and M. Zhu, "Mobile video object detection with temporally-aware feature maps," 2018, pp. 5686–5695.
- [30] B. Zhao, B. Zhao, L. Tang, Y. Han, and W. Wang, "Deep spatial-temporal joint feature representation for video object detection," *Sensors*, vol. 18, no. 3, p. 774, 2018.
- [31] H. Zhu, H. Wei, B. Li, X. Yuan, and N. Kehtarnavaz, "A review of video object detection: Datasets, metrics and methods," *Applied Sciences*, vol. 10, no. 21, p. 7834, 2020.
- [32] R. Gadde, V. Jampani, and P. V. Gehler, "Semantic video cnns through representation warping," 2017, pp. 4453–4462.
- [33] P.-Y. Huang, W.-T. Hsu, C.-Y. Chiu, T.-F. Wu, and M. Sun, "Efficient uncertainty estimation for semantic segmentation in videos," 2018, pp. 520–535.
- [34] S. Jain, X. Wang, and J. E. Gonzalez, "Accel: A corrective fusion network for efficient semantic segmentation on video," 2019, pp. 8866–8875.
- [35] E. Shelhamer, K. Rakelly, J. Hoffman, and T. Darrell, "Clockwork convnets for video semantic segmentation." Springer, 2016, pp. 852–868.
- [36] Y. Li, J. Shi, and D. Lin, "Low-latency video semantic segmentation," 2018, pp. 5997–6005.
- [37] F. Liang, T.-W. Chin, Y. Zhou, and D. Marculescu, "Ant: Adapt network across time for efficient video processing," 2022, pp. 2603–2608.
- [38] P. Hu, F. Caba, O. Wang, Z. Lin, S. Sclaroff, and F. Perazzi, "Temporally distributed networks for fast video semantic segmentation," 2020, pp. 8818–8827.
- [39] Y. Liu, C. Shen, C. Yu, and J. Wang, "Efficient semantic video segmentation with per-frame inference." Springer, 2020, pp. 352–368.
- [40] —, "Efficient video segmentation models with per-frame inference," *arXiv:2202.12427*, 2022.
- [41] A. Habibian, H. Ben Yahia, D. Abati, E. Gavves, and F. Porikli, "Delta distillation for efficient video processing." Springer, 2022, pp. 213–229.
- [42] X. Zhu, Y. Wang, J. Dai, L. Yuan, and Y. Wei, "Flow-guided feature aggregation for video object detection," 2017, pp. 408–417.
- [43] G. Bertasius, L. Torresani, and J. Shi, "Object detection in video with spatiotemporal sampling networks," 2018, pp. 331–346.
- [44] H. Wu, Y. Chen, N. Wang, and Z. Zhang, "Sequence level semantics aggregation for video object detection," 2019, pp. 9217–9225.
- [45] Y. Chen, Y. Cao, H. Hu, and L. Wang, "Memory enhanced global-local aggregation for video object detection," 2020, pp. 10337–10346.
- [46] J. Martinez, R. Hossain, J. Romero, and J. J. Little, "A simple yet effective baseline for 3d human pose estimation," 2017, pp. 2640–2649.
- [47] G. Gkioxari, A. Toshev, and N. Jaitly, "Chained predictions using convolutional neural networks." Springer, 2016, pp. 728–743.
- [48] M. Lin, L. Lin, X. Liang, K. Wang, and H. Cheng, "Recurrent 3d pose sequence machines," 2017, pp. 810–819.
- [49] B. Artacho and A. Savakis, "Unipose: Unified human pose estimation in single images and videos," 2020, pp. 7035–7044.
- [50] T. Pfister, J. Charles, and A. Zisserman, "Flowing convnets for human pose estimation in videos," 2015, pp. 1913–1921.
- [51] B. Xiao, H. Wu, and Y. Wei, "Simple baselines for human pose estimation and tracking," 2018, pp. 466–481.
- [52] D. Pavllo, C. Feichtenhofer, D. Grangier, and M. Auli, "3d human pose estimation in video with temporal convolutions and semi-supervised training," 2019, pp. 7753–7762.
- [53] Z. Liu, H.-J. Wang, Z. Xu, T. Darrell, and E. Shelhamer, "Confidence adaptive anytime pixel-level recognition," 2022.
- [54] L. Bazzani, N. de Freitas, H. Larochelle, V. Murino, and J.-A. Ting, "Learning attentional policies for tracking and recognition in video with deep networks," 2011.
- [55] M. Denil, L. Bazzani, H. Larochelle, and N. de Freitas, "Learning where to attend with deep architectures for image tracking," *Neural Computation*, vol. 24, no. 8, pp. 2151–2184, 2012.
- [56] H. Rhee, D. Min, S. Hwang, B. Andreis, and S. J. Hwang, "Distortion-aware network pruning and feature reuse for real-time video segmentation," *arXiv:2206.09604*, 2022.
- [57] A. Habibian, D. Abati, T. S. Cohen, and B. E. Bejnordi, "Skip-convolutions for efficient video processing," 2021, pp. 2695–2704.
- [58] Y. Chai, "Patchwork: A patch-wise attention network for efficient object detection and segmentation in video streams," 2019, pp. 3415–3424.
- [59] B. Ehteshami Bejnordi, A. Habibian, F. Porikli, and A. Ghodrati, "Salisa: Saliency-based input sampling for efficient video object detection." Springer, 2022, pp. 300–316.
- [60] Z. Huang, S. Bai, and J. Z. Kolter, "(Implicit)²: Implicit layers for implicit representations," 2021.
- [61] S. Bai, V. Koltun, and J. Z. Kolter, "Neural deep equilibrium solvers," 2021.
- [62] A. Pal, A. Edelman, and C. Rackauckas, "Mixing implicit and explicit deep learning with skip deqs and infinite time neural odes (continuous deqs)," *arXiv:2201.12240*, 2022.
- [63] S. Bai, Z. Geng, Y. Savani, and J. Z. Kolter, "Deep equilibrium optical flow estimation," 2022, pp. 620–630.
- [64] C. Lu, J. Chen, C. Li, Q. Wang, and J. Zhu, "Implicit normalizing flows," 2021.
- [65] L. Ma, T. Wang, B. Dong, J. Yan, X. Li, and X. Zhang, "Implicit feature refinement for instance segmentation," in *Proc. 29th ACM Int. Conf. Multimedia*, 2021, pp. 3088–3096.
- [66] T. Wang, X. Zhang, and J. Sun, "Implicit feature pyramid network for object detection," *arXiv:2012.13563*, 2020.
- [67] S. Bai, V. Koltun, and J. Z. Kolter, "Stabilizing equilibrium models by jacobian regularization," 2021.
- [68] Z. Geng, X.-Y. Zhang, S. Bai, Y. Wang, and Z. Lin, "On training implicit models," vol. 34, pp. 24247–24260, 2021.
- [69] S. W. Fung, H. Heaton, Q. Li, D. McKenzie, S. Osher, and W. Yin, "Jfb: Jacobian-free backpropagation for implicit networks," 2022.
- [70] S. Bai, J. Z. Kolter, and V. Koltun, "Trellis networks for sequence modeling," 2019.
- [71] M. Dehghani, S. Gouws, O. Vinyals, J. Uszkoreit, and L. Kaiser, "Universal transformers," 2019.
- [72] O. Russakovsky, J. Deng, H. Su, J. Krause, S. Satheesh, S. Ma, Z. Huang, A. Karpathy, A. Khosla, M. Bernstein, A. C. Berg, and L. Fei-Fei, "ImageNet Large Scale Visual Recognition Challenge," vol. 115, no. 3, pp. 211–252, 2015.
- [73] L. Van der Maaten and G. Hinton, "Visualizing data using t-sne." *Journal of machine learning research*, vol. 9, no. 11, 2008.
- [74] A. Paszke, S. Gross, F. Massa, A. Lerer, J. Bradbury, G. Chanan, T. Killeen, Z. Lin, N. Gimelshein, L. Antiga, A. Desmaison, A. Kopf, E. Yang, Z. DeVito, M. Raison, A. Tejani, S. Chilamkurthy, B. Steiner, L. Fang, J. Bai, and S. Chintala, "Pytorch: An imperative style, high-performance deep learning library," 2019, pp. 8024–8035.
- [75] M. Cordts, M. Omran, S. Ramos, T. Rehfeld, M. Enzweiler, R. Benenson, U. Franke, S. Roth, and B. Schiele, "The cityscapes dataset for semantic urban scene understanding," 2016.
- [76] K. Chen, J. Wang, J. Pang, Y. Cao, Y. Xiong, X. Li, S. Sun, W. Feng, Z. Liu, J. Xu, Z. Zhang, D. Cheng, C. Zhu, T. Cheng, Q. Zhao, B. Li, X. Lu, R. Zhu, Y. Wu, J. Dai, J. Wang, J. Shi, W. Ouyang, C. C. Loy, and D. Lin, "MMDetection: Open mmlab detection toolbox and benchmark," *arXiv:1906.07155*, 2019.
- [77] M. Contributors, "MMTracking: OpenMMLab video perception toolbox and benchmark." <https://github.com/open-mmlab/mtracking>, 2020.
- [78] J. Deng, Y. Pan, T. Yao, W. Zhou, H. Li, and T. Mei, "Relation distillation networks for video object detection," 2019, pp. 7023–7032.
- [79] S. Ren, K. He, R. Girshick, and J. Sun, "Faster r-cnn: Towards real-time object detection with region proposal networks," vol. 28, 2015.
- [80] T.-Y. Lin, P. Dollár, R. Girshick, K. He, B. Hariharan, and S. Belongie, "Feature pyramid networks for object detection," 2017, pp. 2117–2125.
- [81] M. Andriluka, L. Pishchulin, P. Gehler, and B. Schiele, "2d human pose estimation: New benchmark and state of the art analysis," June 2014.
- [82] M. Contributors, "Openmmlab pose estimation toolbox and benchmark," <https://github.com/open-mmlab/mmpose>, 2020.
- [83] D. C. Luvizon, D. Picard, and H. Tabia, "2d/3d pose estimation and action recognition using multitask deep learning," 2018, pp. 5137–5146.
- [84] K. Sun, B. Xiao, D. Liu, and J. Wang, "Deep high-resolution representation learning for human pose estimation," 2019, pp. 5693–5703.
- [85] J. Wang, K. Sun, T. Cheng, B. Jiang, C. Deng, Y. Zhao, D. Liu, Y. Mu, M. Tan, X. Wang *et al.*, "Deep high-resolution representation learning for visual recognition," vol. 43, no. 10, pp. 3349–3364, 2020.

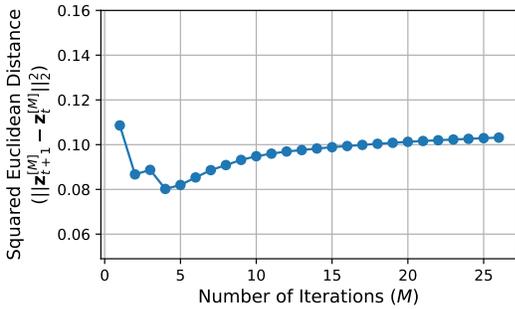


Fig. 15: Squared Euclidean distance of two consecutive frames’ iteration processes throughout all iterations.

APPENDIX

A. Overview

In the supplementary material we present further experimental results on StreamDEQ’s convergence and compare IL-StreamDEQ and (S)UR-StreamDEQ on video object detection and human pose estimation in videos. Furthermore, we provide in-depth qualitative results on video semantic segmentation. Finally, we explore shot changes where there is a sudden change in the video using semantic segmentation.

B. Further Empirical Results on StreamDEQ Convergence

To support our results regarding the asymptotic behavior of StreamDEQ, we present an additional empirical result on the similarity of representation inference paths across the consecutive video frames. For this purpose, we measure the squared Euclidean distance of pairs of consecutive frame representations as found by the Broyden solver for each M value, starting from zero initializations, across the entire dataset.

The results are shown in Fig. 15. We first observe that the distance values are unstable for small M values, which is not surprising as we already know that from-scratch DEQ inference requires a *sufficiently large* number of iterations. More importantly, for larger M values ($M \geq 15$), we observe that distance values start to converge towards 0.1, which is compatible with our observations in Fig. 3 from the main paper.

Now, we present a comparison of two different initialization schemes for IL-StreamDEQ. We show the first scenario in the main paper that is the original version of IL-StreamDEQ (Eq. (6) from the main paper) where the representations are initially zero and as the videos progress, the representation quality improves. The second scenario corresponds to Eq. (5) from the main paper, where we use the reference representations of the first frame to initialize the solver and apply IL-StreamDEQ then on. Results of this experiment in Fig. 16 show that as the offset of the evaluated frame increases, mIoU starts decreasing, which is expected because the further we move away from the first frame, the more irrelevant its representation will become. However, mIoU then stabilizes at a value proportional to the number of Broyden iterations (the more iterations, the better

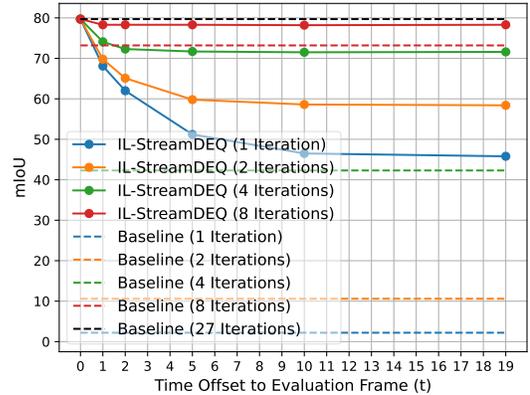


Fig. 16: IL-StreamDEQ semantic segmentation results (in mIoU) on the Cityscapes dataset as a function of solver iterations when the first frame representation is initialized with the reference representation.

the mIoU). This shows that IL-StreamDEQ is able to extract improved features over time. IL-StreamDEQ’s performance with 8 iterations is still comparable with the baseline (MDEQ) with 27 iterations. Comparing this experiment to the original IL-StreamDEQ scheme in the main paper, the convergence of mIoU scores towards similar values suggests again that the effect of the first frame’s representation diminishes as we move away from the initial point.

C. Comparison Between IL-StreamDEQ and (S)UR-StreamDEQ

We present the results of IL-StreamDEQ and UR-StreamDEQ on video object detection in Fig. 17 and Fig. 18, respectively. We observe the same trends with the segmentation task from the main paper. Over time, the detection performance increases and stabilizes at a value proportional to the number of Broyden iterations or unrollings.

We note that neither IL-StreamDEQ nor UR-StreamDEQ cannot produce any detection results in the non-streaming mode with 1 or 2 iterations. In streaming mode, if we perform 2 iterations with IL-StreamDEQ, we improve the performance from 0 to 39.5 mAP@50 in 20 frames.

Again, SUR-StreamDEQ outperforms UR-StreamDEQ for low number of unrollings. UR-StreamDEQ does not perform well initially for 1 unrolling per frame and is only able to produce good representations after ~ 10 frames. This is closer to what we see with IL-StreamDEQ in terms of performance.

We also experiment using IL-StreamDEQ and UR-StreamDEQ to estimate human poses in videos whose results we give in Fig. 19 and Fig. 20, respectively.

The results of these experiments again align with our previous experiments, in that, for all 3 versions of StreamDEQ, we see that the performance of the model improves rapidly after the first few frames. Overall, IL-StreamDEQ performs the worst and SUR-StreamDEQ performs the best. Still, IL-StreamDEQ obtains 84.7 PCKh and 85.7 PCKh with 4 and

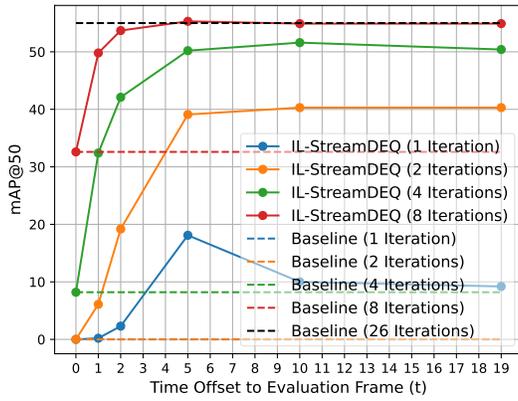


Fig. 17: mAP@50 results of IL-StreamDEQ for various number of iterations after initialization with zeros from the beginning of a clip on the ImageNet-VID dataset.

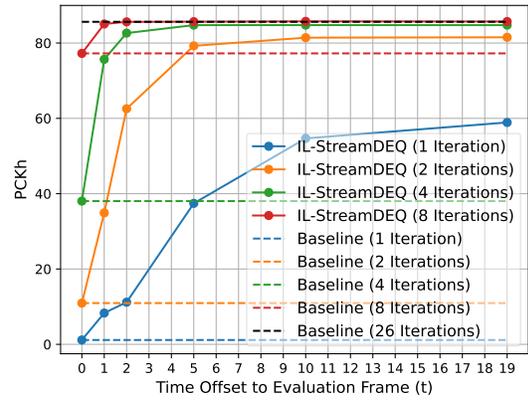


Fig. 19: PCKh results of IL-StreamDEQ for various number of iterations after initialization with zeros from the beginning of a clip on the MPII dataset.

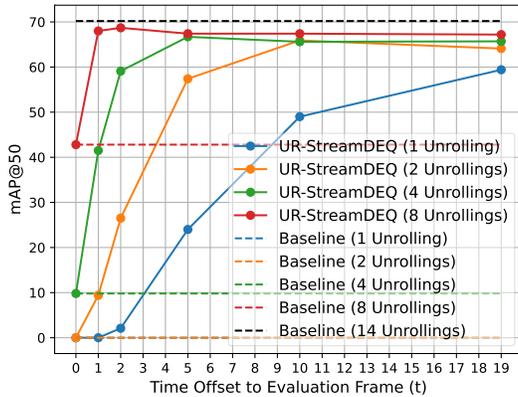


Fig. 18: mAP@50 results of UR-StreamDEQ for various number of iterations after initialization with zeros from the beginning of a clip on the ImageNet-VID dataset.

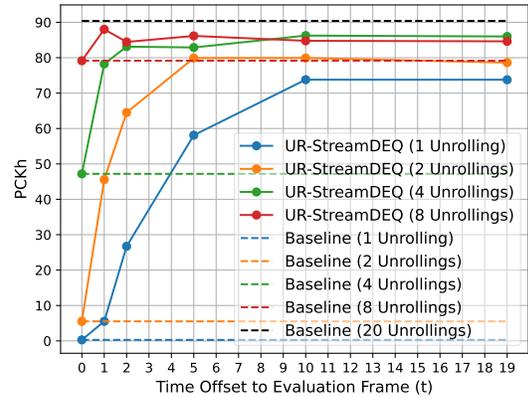


Fig. 20: PCKh results of UR-StreamDEQ for various number of iterations after initialization with zeros from the beginning of a clip on the MPII dataset.

8 iterations per frame, respectively, matching its single-frame performance of 85.7 PCKh.

UR-StreamDEQ brings an advantage for low numbers of iterations compared to IL-StreamDEQ with its 1 iteration per frame performance being 73.8 PCKh. However, we see a slight drop of performance when we perform 8 iterations per frame after the first couple of frames. We made a similar observation in Fig. 18 and we again suggest that this occurs due to UR-StreamDEQ not having seen representations of different complexities and therefore, is not able to adapt perfectly when it encounters a situation where too many iterations are performed. Yet, its performance drop is not significant where it is able to almost match the performance of the 4 iterations per frame case (86.0 PCKh) at 84.6 PCKh.

Again due to the stochasticity we introduce to SUR-StreamDEQ, it produces predictions with over 50 PCKh after the first frame for all numbers of iterations. Furthermore, performing 4 iterations per frame versus 8 iterations per frame only makes a small difference as the performance saturates at about 90 PCKh for SUR-StreamDEQ. Finally, even when we

perform 1 iteration at each frame, SUR-StreamDEQ obtains 79.6 PCKh which is comparable with the performance of the other StreamDEQ versions when we perform 2 iterations at each frame.

D. Shot Change Experiments

We study the effects of shot changes using IL-StreamDEQ where we effectively connect two different clips together. To simulate this behavior, we initialize the solver with the reference representations from a random frame from either the Cityscapes dataset or the ImageNet-VID dataset and run IL-StreamDEQ starting from the representations of that frame. We present the results of Cityscapes to Cityscapes shot change experiments in Fig. 21 and ImageNet-VID to Cityscapes shot change experiments in Fig. 22. The former of these experiments is simpler as the representations in two different videos from the same dataset are likely to be more similar. We notice that, for shot changes in similar contexts, *i.e.* Cityscapes to Cityscapes, the mIoU scores on initial frames are higher than our previous experiments presented in the main paper in Fig.

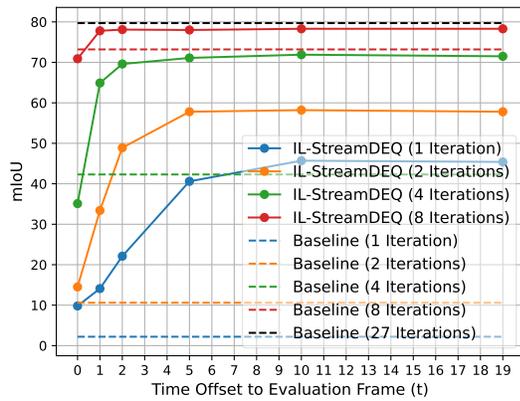


Fig. 21: mIoU results of IL-StreamDEQ with shot changes from the Cityscapes dataset.

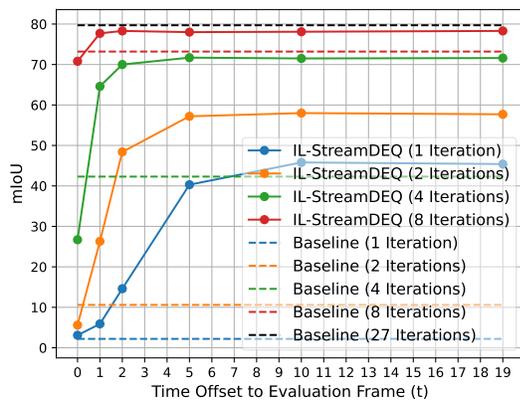


Fig. 22: mIoU results of IL-StreamDEQ with shot changes from the ImageNet-VID dataset.

9 and also higher than the ImageNet-VID to Cityscapes shot change scenario in Fig. 22. However, after the first few frames are processed, following a similar trajectory to our previous experiments, mIoU scores stabilize at a value close to our original experiment. We conclude that, even with occasional shot changes, our method is able to adapt to the new scene in a few frames.

E. Qualitative Results

Finally, we illustrate the results of IL-StreamDEQ qualitatively in Fig. 23 with more depth considering different numbers of iterations. For 1 iteration, while the baseline cannot produce any meaningful segmentation, IL-StreamDEQ starts capturing many segments correctly at the 4th frame. With 2 iterations, while the DEQ baseline still produces poor results, IL-StreamDEQ starts to yield accurate predictions in early frames compared to the single iteration case. With 4 iterations, while both models provide rough but relevant predictions in the first frame, IL-StreamDEQ predictions start to become clearly more accurate in the following frames; for example, tree trunks and the sky become visible only when IL-StreamDEQ is applied.

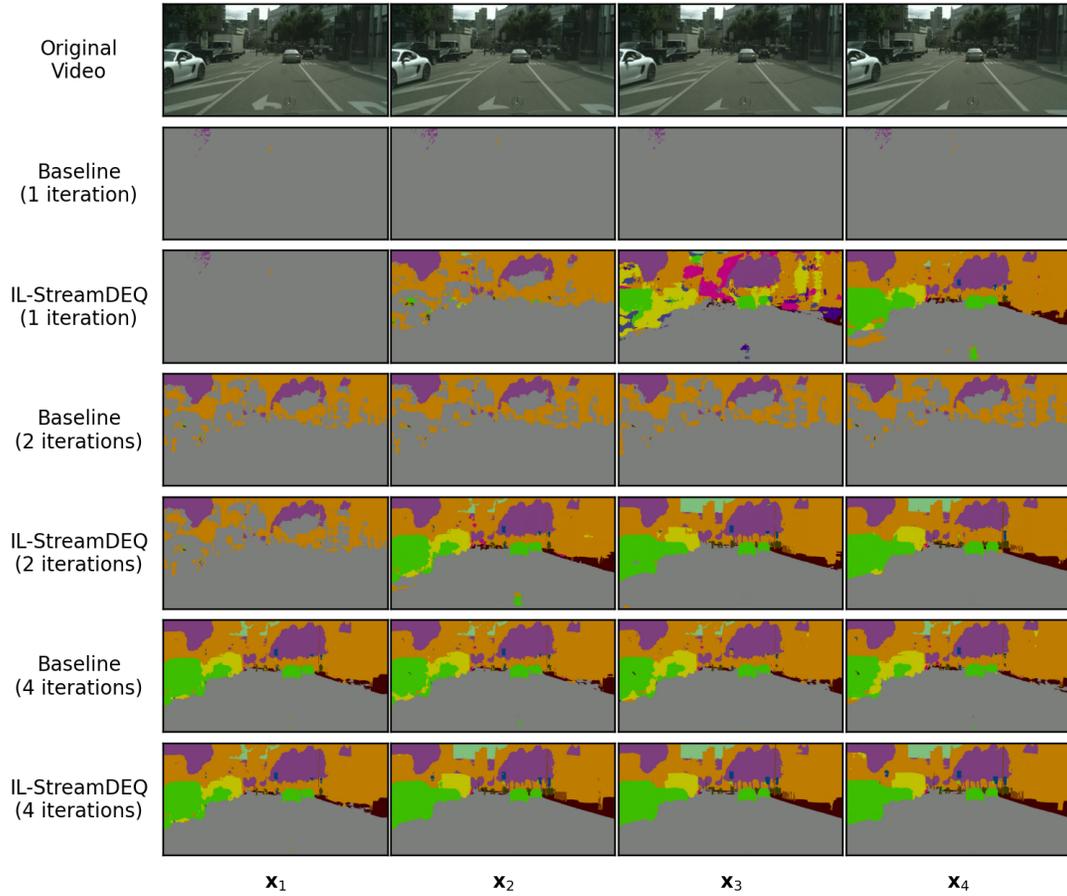


Fig. 23: Qualitative comparison of the baseline with IL-StreamDEQ with different numbers of iterations on the Cityscapes dataset.